Formation and structural transformation of the nonequilibrium phases in the Ru–Ta system induced by ion beam mixing

2006 J. Phys.: Condens. Matter 18 9911

(http://iopscience.iop.org/0953-8984/18/43/012)

INSTITUTE OF PHYSICS PUBLISHING JOURNAL OF PHYSICS: CONDENSED MATTER

J. Phys.: Condens. Matter **18** (2006) 9911–9916 doi:10.1088/0953-8984/18/43/012

Formation and structural transformation of the nonequilibrium phases in the Ru–Ta system induced by ion beam mixing

W C Wang, Y X Shen, J H Li, X Y Li and B X Liu[1]

Advanced Materials Laboratory, Department of Materials Science and Engineering, Tsinghua University, Beijing 100084, People's Republic of China

E-mail: dmslbx@tsinghua.edu.cn.

Received 10 July 2006, in final form 26 September 2006
Published 13 October 2006
Online at stacks.iop.org/JPhysCM/18/9911

Abstract

A Gibbs free energy diagram of the Ru–Ta system is derived from Miedema's theory, which predicts that the metallic glass forming range of the system is within 25–55 at.% of Ta. The unique amorphous alloys are produced for the $Ru_{75}Ta_{25}$, $Ru_{65}Ta_{35}$, $Ru_{57}Ta_{43}$ and $Ru_{50}Ta_{50}$ multilayers upon ion irradiation, matching well with the predicted glass forming range. However, for the $Ru_{43}Ta_{57}$ multilayer, a mixing microstructure consisting of the amorphous and crystalline phases is obtained. Besides, an interesting phenomenon is observed for the $Ru_{25}Ta_{75}$ multilayer, i.e. the transient fcc-Ru and fcc-Ta are first formed respectively from the original hcp-Ru and bcc-Ta upon irradiation and then a unique fcc-$Ru_{25}Ta_{75}$ phase is eventually formed from the transient fcc-Ru and fcc-Ta upon further irradiation. A brief discussion of the experimental results is presented based on the *ab initio* calculations.

In 1960, by using liquid melt quenching, Duwez *et al* obtained the first amorphous Au–Si alloy [1–3]. Since amorphous alloys and metastable crystalline alloys are expected to have novel properties in many aspects, great effort has been made to develop nonequilibrium materials processing techniques [4]. In the early 1980s, ion beam mixing (IBM) of multiple metal layers was introduced to synthesize new nonequilibrium alloys. Because of the effective cooling speed of the IBM [5], a variety of amorphous alloys and metastable alloys has been produced so far, in miscible systems as well as in immiscible systems [6]. For binary alloy systems under irradiation, two main dynamic mechanisms are encountered, i.e. the imposed ion mixing mechanism (IMM) and the thermally driven mechanism (TDM). For an immiscible binary alloy, the two mechanisms drive the alloy in opposition, i.e. IMM conducing phase homogenization and TDM inducing phase separation. The phase transformation process and

[1] Author to whom any correspondence should be addressed.

the resultant depend on the competition of the two mechanisms. In the framework of Martin's theoretical basis for describing the competition [7], Enrique and Bellon proposed a continuum model [8, 9], which has been employed successfully to interpret the phase transformation and has been verified to be useful by molecular dynamics and Monte Carlo simulations [10] as well as experimental results [11]. For miscible alloy systems, especially for those systems with very negative formation enthalpy, the two mechanisms act in conjunction, both driving the alloy into the homogeneous phase. It is shown that the thermodynamic model can be effective in interpreting this type of phase transformation [6]. Besides, *ab initio* calculations have also been applied to explain the competition among different structures in phase transformation [12, 13].

Due to possessing some unique properties, the metastable Ru–Ta alloys have been applied extensively in industry. For example, metastable Ru–Ta compounds have been used in bubble jet printers [14] and Ru–Ta amorphous film has been used in perpendicular magnetic recording systems as the buffer layer [15]. However, the formation and structural transformation of the nonequilibrium phases in the system is still not clear. Consequently, it is necessary to further investigate the phase transition process involved in the Ru–Ta system. In the present work, we first performed the thermodynamic calculations based on Miedema's theory and then conducted an IBM experiment, in order to investigate the formation and structural transformation of the nonequilibrium phases in the Ru–Ta system. Besides, *ab initio* calculations were carried out to explain the structural transformation. Concerning the calculation details, the readers are referred to some recent publications of the authors' group [6].

Now we present the thermodynamic results. Figure 1(a) is the calculated Gibbs free energy diagram of the Ru–Ta system based on Miedema's theory. One can see from figure 1(a) that, when the composition falls into the range 25–55 at.% of Ta, the Gibbs free energy of the amorphous phase is lower than that of the corresponding initial multilayer and the solid solution. It can thus be concluded that the saturated solid solution would become unstable and transform into the corresponding amorphous states when it falls into the composition range. Therefore, the glass-formation range of the Ru–Ta system is estimated to be around 25–55 at.% of Ta.

In order to verify the thermodynamic predications, an IBM experiment was subsequently conducted. In the present experiment, 200 keV Xe^+ ions were applied to the multilayered Ru–Ta samples. Six sets of multilayered Ru–Ta samples were designed with compositions of $Ru_{75}Ta_{25}$, $Ru_{65}Ta_{35}$, $Ru_{57}Ta_{43}$, $Ru_{50}Ta_{50}$, $Ru_{43}Ta_{57}$ and $Ru_{25}Ta_{75}$. Each multilayered sample had a total thickness of about 40 nm, designed to match the TRIM code's calculated projected range plus the projected range straggling [16] of 200 keV Xe^+ ions. The multilayers were prepared by alternately depositing pure Ru (99.9%) and Ta (99.9%) at a rate of 0.5 Å s^{-1} onto a NaCl single-crystal substrate in an electron-gun evaporation system with a vacuum level of 10^{-6} Pa. The as-deposited samples were then irradiated by 200 keV Xe^+ ions in an implanter with a vacuum level better than 5×10^{-4} Pa, and the irradiation doses were in the range from 6×10^{14} Xe^+ cm^{-2} to 9×10^{15} Xe^+ cm^{-2}. The sample holder was cooled by liquid nitrogen (77 K) during the irradiation, and the xenon ion current density was confined to be about 2 μA cm^{-2} to minimize the heating effect. For structural characterization, a bright-field examination and selected area diffraction (SAD) analysis on room-temperature transmission electron microscopy (JEOL JEM 200 CX, operated at 160 keV accelerating voltage) was performed. For the determination of the composition of the as-deposited films and the resultant alloy phases in the films, energy dispersive spectroscopy (EDS) was employed. The life-time during EDS analysis was about 10 min. For each sample, at least ten points were analysed. High-resolution TEM was also used in the experiment.

For the $Ru_{75}Ta_{25}$ multilayered samples, figure 2 shows typical selected area diffraction (SAD) patterns of the as-deposited sample and its irradiated states at doses of 6×10^{14}, 5×10^{15},

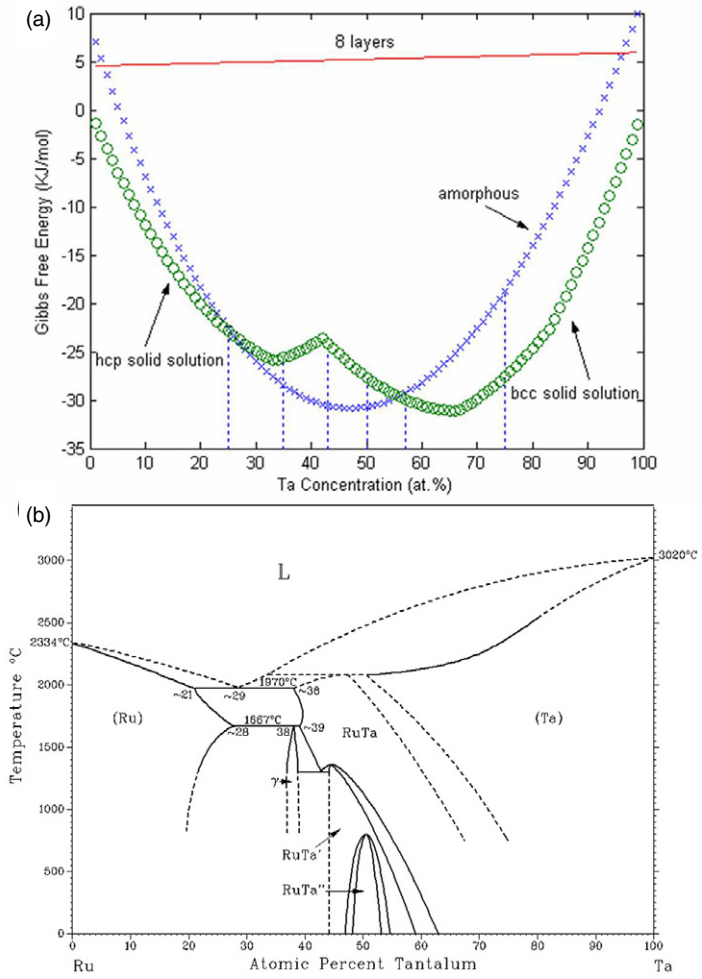

Figure 1. The Gibbs free energy diagram derived from Miedema's theory (a) and the phase diagram (b) of the Ru–Ta system.

(This figure is in colour only in the electronic version)

and 9×10^{15} Xe^{+} cm^{-2}. The sharp diffraction rings of polycrystalline hcp-Ru and bcc-Ta in figure 2(a) suggest that Ru and Ta in the as-deposited state were not mixed and were most likely located in the separated Ru layers and Ta layers. When the irradiation dose was above 5×10^{15} Xe^{+} cm^{-2}, some diffraction lines from hcp-Ru and bcc-Ta gradually got widened, as shown in figures 2(b) and (c). When the irradiation dose is up to 9×10^{15} Xe^{+} cm^{-2}, the diffraction lines were transformed into some diffuse halos, as shown in figure 2(d), indicating the formation of a unique amorphous phase. A high-resolution image of the amorphous phase is shown in figure 2(e). Similar structural transitions were observed for the $Ru_{65}Ta_{35}$, $Ru_{57}Ta_{43}$ and $Ru_{50}Ta_{50}$ multilayered samples, but the irradiation doses for amorphization were different. For the $Ru_{43}Ta_{57}$ sample, there was only a partial amorphous phase, i.e. an amorphous and a crystalline phase coexisting, at an irradiation dose of 9×10^{15} Xe^{+} cm^{-2}. From the analysis above, one can see that the experimental results are generally consistent with the thermodynamic predictions.

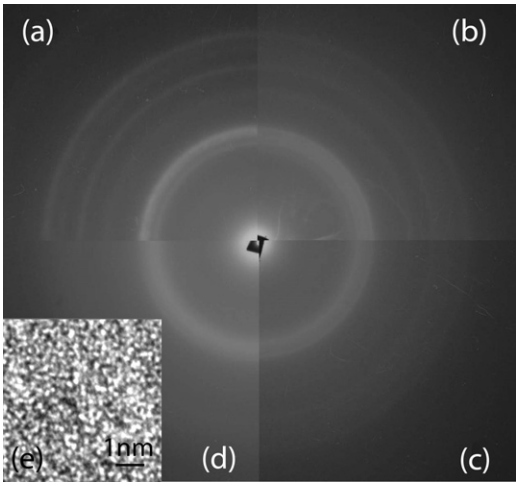

Figure 2. Selected area diffraction patterns for $Ru_{75}Ta_{25}$ multilayers with eight layers: as-deposited state (a), irradiated states at an irradiation dose of 6×10^{14} Xe^+ cm^{-2} (b), 5×10^{15} Xe^+ cm^{-2} (c), 9×10^{15} Xe^+ cm^{-2} (d), and a high-resolution image of the amorphous phase at an irradiation dose of 9×10^{15} Xe^+ cm^{-2} (e).

Interestingly, no amorphization was observed for the $Ru_{25}Ta_{75}$ sample; figure 3 exhibits the SAD patterns under different irradiation doses. It can be seen from figure 3 that two metastable fcc phases were formed and remained until the irradiation dose was up to 5×10^{15} Xe^+ cm^{-2}. From figure 3, it can also be seen that a structural transition from the two fcc phases into one new fcc phase took place when the irradiation dose was above 5×10^{15} Xe^+ cm^{-2}, and that the newly formed fcc phase would not change even at an irradiation dose of 9×10^{15} Xe^+ cm^{-2}. For the phase transformation of $Ru_{25}Ta_{75}$, at a low irradiation dose of less than 6×10^{14} Xe^+ cm^{-2}, the Ru in the $Ru_{25}Ta_{75}$ multilayered sample experiences a transition from hcp structure into fcc structure with a sliding of the $(0002)_{hcp}$ plane atoms along the $\frac{1}{3}\langle 1\bar{1}00\rangle_{hcp}$ vector direction. The lattice constant relationship between the two structures can easily be determined to be $a_{fcc} = \sqrt{2}a_{hcp}$. Meanwhile, the Ta in the sample transforms from bcc structure to fcc structure through a two-step shearing mechanism of bcc- > hcp- > fcc. The lattice constant relationship in the first shearing step from bcc structure into hcp structure can be determined to be $a_{hcp} = \frac{\sqrt{3}}{2}a_{bcc}$ and $c_{hcp} = \sqrt{2}a_{bcc}$, where $(111)_{bcc}$ acts as the habit plane and $\langle \bar{1}1\bar{1}\rangle_{bcc}$ acts as the shear axis. The lattice constant relationship in the second shearing step from hcp structure into fcc structure is just the same as the one mentioned above. The lattice constant of the fcc-Ta phase is therefore $a_{fcc} = \frac{\sqrt{6}}{2}a_{bcc}$. In this sense, two fcc metastable phases, i.e. fcc-Ru and fcc-Ta, can be observed at low irradiation doses. With the relationships mentioned above, the lattice constants of these two fcc phases were calculated. Table 1 lists both the calculated and the experimental lattice constants. The difference between the calculated and the experimentally observed lattice constants is just less than 0.5%. However, the fcc-Ru phase and the fcc-Ta phase are not stable. At irradiation doses from 6×10^{14} Xe^+ cm^{-2} to 9×10^{15} Xe^+ cm^{-2}, they were observed to have transformed into a new fcc phase, as described above.

To give an energetic explanation, we have calculated the lattice constants and the total energy of hcp-Ru, bcc-Ta, fcc-Ru, fcc-Ru and fcc-$Ru_{25}Ta_{75}$ by performing *ab initio* calculations using CASTEP [18]. In the calculations, the $4d^75s^1$ and $5d^36s^2$ pseudo-atomic configurations were adopted for Ru and Ta, respectively. For a description of the exchange and correlation energy, the generalized-gradient approximation (GGA) of Perdew–Wang [19] was used. The

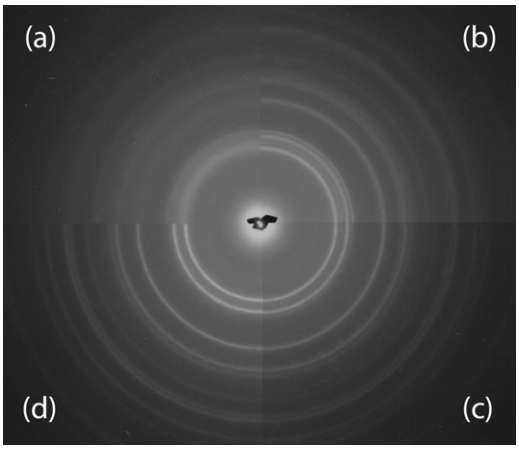

Figure 3. Selected area diffraction patterns for $Ru_{25}Ta_{75}$ multilayers with seven layers: as-deposited state (a), and the irradiated state at irradiation doses of 6×10^{14} Xe^{+} cm^{-2} (b), 1×10^{15} Xe^{+} cm^{-2} (c) and 5×10^{15} Xe^{+} cm^{-2} (d).

Table 1. The lattice constants (Å) of hcp-Ru, bcc-Ta and metastable fcc-Ru, fcc-Ta in the experiment, along with the calculated lattice constants.

	Experiment[a]	Our work	Calculated
hcp-Ru	$a = 2.7059$		
	$c = 4.2818$		
bcc-Ta	$a = 3.2980$		
fcc-Ru		$a = 3.81$	$a = 3.826$
fcc-Ta		$a = 4.04$	$a = 4.0392$

[a] Reference [17].

Table 2. The lattice constant (a), total energy (H), formation energy (H^{For}) and of Ru, Ta and $Ru_{25}Ta_{75}$ determined by *ab initio* calculation.

	a (Å)	H (eV/atom)	H^{For} (eV/atom)
hcp-Ru	$a = 2.7209$	−2608.5115	0
	$c = 4.2818$		
bcc-Ta	$a = 3.2547$	−139.9671	0
fcc-Ru	$a = 3.8104$	−2608.3990	0.1125
fcc-Ta	$a = 4.0490$	−139.6099	0.3662
fcc-$Ru_{25}Ta_{75}$ [a]	$a = 4.0535$	−756.9645	ΔH_1 [b] 0.1387
			ΔH_2 [c] −0.1573

[a] fcc-$Ru_{25}Ta_{75}$: phase with fcc structure ($L1_2$ structure).
[b] ΔH_1: stands for the energy difference between fcc-$Ru_{25}Ta_{75}$ and hcp-Ru, bcc-Ta, expressed by $\Delta H_1 = H_{\text{fcc-}Ru_{25}Ta_{75}} - 0.25H_{\text{hcp-Ru}} - 0.75H_{\text{bcc-Ta}}$.
[c] ΔH_2: stands for the energy difference between fcc-$Ru_{25}Ta_{75}$ and fcc-Ru, fcc-Ta, expressed by $\Delta H_2 = H_{\text{fcc-}Ru_{25}Ta_{75}} - 0.25H_{\text{fcc-Ru}} - 0.75H_{\text{fcc-Ta}}$.

integration in the Brillouin zone (BZ) is performed on the special κ points determined from the Monkhorst–Pack scheme [20] and geometry optimization is conducted using the Broyden–Fletcher–Goldfarb–Shanno (BFGS) method [21]. Table 2 lists the calculated results, from which the fcc-$Ru_{25}Ta_{75}$ phase presents a lower energy than that of the mixture of fcc-Ru and fcc-Ta, indicating that the fcc-Ru and fcc-Ta mixture would transform into an fcc-$Ru_{25}Ta_{75}$

phase upon further irradiation. Moreover, by calculating ΔH_1 (the energy difference between fcc-$Ru_{25}Ta_{75}$ and the mixture of hcp-Ru and bcc-Ta) and ΔH_2 (the energy difference between fcc-$Ru_{25}Ta_{75}$ and the mixture of fcc-Ru and fcc-Ta), which are also listed in table 2, we can see that, since $\Delta H_1 > 0$ and $\Delta H_2 < 0$, fcc-$Ru_{25}Ta_{75}$ favours forming from a mixture of fcc-Ru and fcc-Ta instead of a mixture of hcp-Ru and bcc-Ta.

In summary, a Gibbs free energy diagram of the Ru–Ta system has been derived from Miedema's theory, which predicts that the metallic glass forming range of the system is within 25–55 at.% of Ta. The unique amorphous phases in the $Ru_{75}Ta_{25}$, $Ru_{65}Ta_{35}$, $Ru_{57}Ta_{43}$, $Ru_{50}Ta_{50}$ multilayered samples and an amorphous phase coexisting with a crystalline phase in the $Ru_{43}Ta_{57}$ sample were formed by IBM. At the alloy composition of $Ru_{25}Ta_{75}$, two transient phases, i.e. fcc-Ru and fcc-Ta, were formed at an irradiation dose lower than 6×10^{14} Xe^{+} cm^{-2}, and they transformed into an fcc-$Ru_{25}Ta_{75}$ phase upon further irradiation.

Acknowledgments

The authors are grateful for financial support from the National Natural Science Foundation of China (50531040), The Ministry of Science and Technology, and Tsinghua University.

References

[1] Klement W, Willens R H and Duwez P 1960 *Nature* **187** 869
[2] Zallen R 1983 *The Physics of Amorphous Solids* (New York: Wiley)
[3] Greer A L 1995 *Science* **267** 1947
[4] Lu Y Q, Zhu Y Y, Chen Y F, Zhu S N, Ming N B and Feng Y J 1999 *Science* **284** 1822
[5] Thompson M W 1969 *Defects and Radiation Damage in Metals* (Cambridge: Cambridge University Press)
[6] Liu B X, Lai W S and Zhang Z J 2001 *Adv. Phys.* **50** 367
[7] Martin G 1984 *Phys. Rev.* B **30** 1424
[8] Enrique R and Bellon P 2000 *Phys. Rev. Lett.* **84** 2885
[9] Enrique R A and Bellon P 2001 *Phys. Rev.* B **63** 134111
[10] Enrique R A, Nodlund K, Averback R S and Bellon P 2003 *J. Appl. Phys.* **93** 2917
[11] Wei L C and Averback R S 1997 *J. Appl. Phys.* **81** 613
[12] He X, Kong L T, Li J H, Li X Y and Liu B X 2006 *Acta Mater.* **54** 3375
[13] Alatalo M, Weiner M and Watson R E 1998 *Phys. Rev.* B **57** R2009
[14] Wuu D S, Chan C C and Horng R H 1999 *J. Vac. Sci. Technol.* A **17** 3327
[15] Platt C L, Wierman K W, Svedberg E G, Klemmer T J, Howard J K and Smith D J 2002 *J. Magn. Magn. Mater.* **247** 153
[16] Ziegler J F and Biersack J P 1992 *TRIM* (New York: Pergamon)
[17] Pearson W B 1958 *A Handbook of Lattice Spacing and Structure of Metals and Alloys* (London: Pergamon)
[18] Segall M D, Lindan P L, Probert M J, Pickard C J, Hasnip P J, Clark S J and Payne M C 2002 *J. Phys.: Condens. Matter* **14** 2717
[19] Perdew J P and Wang Y 1992 *Phys. Rev.* B **45** 13244
[20] Monkhorst H J and Pack J D 1976 *Phys. Rev.* B **13** 5188
[21] Fischer T H and Almlof J 1992 *J. Phys. Chem.* **96** 9768